RSC Advances

PAPER

View Article Online
View Journal | View Issue

Cite this: *RSC Adv.*, 2021, **11**, 27720

Photocatalytic degradation of ibuprofen using titanium oxide: insights into the mechanism and preferential attack of radicals†

Maicon Oliveira Miranda,[ab] Wesley Eulálio Cabral Cavalcanti,[a] Felipe Fernandes Barbosa,[a] José Antonio de Sousa,[c] Francisco Ivan da Silva,[d] Sibele B. C. Pergher[a] and Tiago Pinheiro Braga *[a]

The present work studied ibuprofen degradation using titanium dioxide as a photocatalyst. Mechanistic aspects were presented and the preferred attack sites by the OH• radical on the ibuprofen molecule were detailed, based on experimental and simple theoretical-computational results. Although some previous studies show mechanistic proposals, some aspects still need to be investigated, such as the participation of 4-isobutylacetophenone in the ibuprofen degradation and the preferred regions of attack by OH• radicals. The photodegradation was satisfactory using 0.03 g of TiO_2 and pH = 5.0, reaching 100% decontamination in 5 min. The zeta potential curve showed the regions of attraction and repulsion between TiO_2 and ibuprofen, depending on the pH range and charge of the species, influencing the amount of by-products formed. Different by-products have been identified by GC-MS, such as 4-isobutylacetophenone. Ibuprofen conversion to 4-isobutylacetophenone takes place through decarboxylation reaction followed by oxidation. The proposed mechanism indicates that the degradation of ibuprofen undergoes a series of elementary reactions in solution and on the surface. Three different radicals (OH•, $O_2^{-\bullet}$ and OOH•) are produced in the reaction sequence and contribute strongly to the oxidation and mineralization of ibuprofen and by-products, but the hydroxyl radical has a greater oxidation capacity. The simple study using the DFT approach demonstrated that the OH• radical attacks preferentially in the region of the ibuprofen molecule with high electronic density, which is located close to the aromatic ring (C=C bond). The presence of the OH• radical was confirmed through a model reaction using salicylic acid as a probe molecule.

Received 4th June 2021
Accepted 5th August 2021

DOI: 10.1039/d1ra04340d

rsc.li/rsc-advances

1 Introduction

Contaminants or emerging pollutants belong to a group of substances often found in the environment, where their effects are not well known, but they can bring serious risks to the ecosystem.[1] In general, there is no strict legislation to monitor the release of these products into the environment.[2]

Pharmaceutical products, steroids and hormones are some types of water pollutants.[3] The drugs have been found in several aquatic systems in many countries,[4] and their release into the environment occurs mainly through domestic and hospital waste. Considering that the human body is unable to fully metabolize these substances, they were excreted through feces, urine and sweat.[5]

Nonsteroidal anti-inflammatory drugs, designated as NSAIDs, are the most consumed class of drugs in the world because, usually, they do not need a medical prescription. Consequently, they are an important group regarding the contamination environmental impact by drugs. Ibuprofen is among the most widely NSAIDs used on a global scale, and it has been found in several regions of the planet.[6]

Pharmaceutical wastes can easily found in the water system because the vast majority of sewage treatment plants lack the ability to retain or degrade these substances.[7–10] Therefore, it is necessary to develop new methods of removing or deplete these products from the environment. An alternative to this issue is the advanced oxidative processes (AOPs).

The AOPs use the production of oxidants such as hydroxyl (OH•), peroxyl ($O_2^{-\bullet}$) and hydroperoxide ($HO_2^{\bullet}$) radicals to degrade the organic materials and mineralize the contaminant to carbon dioxide and water.[11–14] Heterogeneous photocatalysis

[a]*Laboratório de Peneiras Moleculares (LABPMOL), Programa de Pós-graduação em Química, Universidade Federal do Rio Grande do Norte (UFRN), Av. Sen. Salgado FIlho, Campus Universitário, Lagoa Nova, 59.078-970, Natal, RN, Brazil. E-mail: tiagoquimicaufrn@gmail.com; Tel: +55 84 933422323*

[b]*Instituto Federal de Educação, Ciência e Tecnologia do Piauí (IFPI) Rodovia PI 213, Zona Rural, 64235-000, Cocal, PI, Brazil*

[c]*Universidade Federal do Piauí, UFPI, Campus Universitário Ministro Petrônio Portella, Ininga, 64049-550 Teresina, PI, Brazil*

[d]*Federal Institute of Piauí, IFPI, Rodovia BR 407, 64750-000, Paulistana, PI, Brazil*

† Electronic supplementary information (ESI) available. See DOI: 10.1039/d1ra04340d

is an excellent example of AOPs using light as an irradiation source. One of the best-known photocatalysts is titanium dioxide due to its efficient photoactivity, its electron–hole recombination rate, high stability, low cost, and safety to the environment and humans.[15] When the photocatalyst surface is irradiated, the absorption energy equal to or higher than the band-gap is able to overcome the energetic barrier, promoting an electron from the valence band (VB) to the conduction band (CB) and creating an electron–hole pair.[16] This combination promotes redox reaction on the photocatalyst surface, producing radicals such as hydroxyl species ($OH^{\bullet}$).[17,18] The hydroxyl radical is a strong oxidative agent, but is not selective, thus, it can react with several compound classes. The presence of these radicals initiates a series of reactions capable of oxidizing organic matter, justifying its importance in advanced oxidative processes for environmental decontamination.[19]

The identification of intermediates and mechanism pathway specifying the participation of oxidants radicals are considered fundamental aspects to understand in detail the oxidation process by photocatalysis such as TiO_2.[20] For example, Wang *et al.* investigated the mechanism of TiO_2 and ZnO catalysts applied in the ibuprofen degradation using UV-LED light.[21] Greater degradation was observed using lower pH values. TiO_2 and ZnO photocatalysts were very efficient for ibuprofen degradation in a much shorter time in comparison to H_2O_2, peroxomonosulfate (PMS) and potassium peroxodisulfate (PDS). In the presence of UV irradiation using only H_2O_2, hydrogen peroxide generates hydroxyl radicals that attack the ibuprofen molecule, obtaining 38.93% of degradation in the highest concentration of H_2O_2 and generating different by-products. However, in the presence of PMS and PDS, which have greater redox potential than peroxide, reached 74% and 55% of degradation, respectively. These compounds provide the formation of sulfate ion during the oxidation process that occurs in the photocatalytic degradation mechanism. However, in the presence of TiO_2, the light excites the electrons on the catalyst surface and the generated hydroxyl radical acts as an oxidizing agent against ibuprofen, achieving 100% of degradation. In another work, Wang *et al.*[22] investigated through DFT approach the conversion mechanism of various intermediates and selected the appropriate radicals to degrade Ibuprofen. It was mentioned that the reaction activity of $^{\bullet}NO_2$ with ibuprofen is lower than $OH^{\bullet}$, since the free energy barrier is higher. Furthermore, hydroxylation products can be generated by radical formation and hydrogen abstraction transfer. Thus, O_2 is important in the formation of hydroxylation products, reacting with the free radical intermediate formed by the addition reaction and promoting the formation of the final hydroxylation products. Lin *et al.*[23] applied TiO_2 combined with boron nitride in the photocatalytic ibuprofen degradation and investigated the mechanisms, formation of products and intermediates. The involvement of boronitride in TiO_2 improved the light absorption efficiency, in addition to the specific surface area, consequently improved e^-–h^+ pair separation efficiency. Another interesting fact is that the presence of boron nitride collaborated with the breakdown of Ibuprofen degradation intermediates.

Although some studies describe the different mechanistic steps in the degradation of ibuprofen showing the different possible oxidants radicals and their action in the solution and surface steps,[24–26] insights indicating the preferred oxidant to attack the ibuprofen molecule and the most favorable region of oxidant attack by $OH^{\bullet}$ radical in the functional groups of the ibuprofen structure remains an interesting approach to be investigated. Furthermore, some reaction pathways for ibuprofen degradation need to be further investigated such as the conversion of the 4-isobutylacetophenone intermediate to CO_2 and H_2O.

Theoretical-computational calculations through DFT theory combined with experimental results are interesting tools to understand the interaction between the polluting molecule and oxidants radicals.[26,27] Few studies have investigated the degradation mechanism of ibuprofen using TiO_2-based photocatalysts with the aid of a DFT approach.[22,28] Although there are some studies that detail the mechanism for ibuprofen degradation using experimental and theoretical results, detailed information regarding the preferred oxidant species to degrade ibuprofen and the preferred interaction between the radical and the functional groups present in the structure of ibuprofen using computational approaches remain scarce.

Thus, in the present work, the photocatalytic degradation pathways of ibuprofen are studied by using a combination of experimental and simple computational investigations. In a first part, ibuprofen degradation was evaluated using different experimental conditions of pH and mass combined with some experimental characterizations. In a second part, the different elementary steps in solution and on the surface for the degradation of ibuprofen were proposed, based on the experimental results obtained, showing the formation of by-products and indicating the role of oxidants radicals in the mineralization of ibuprofen. Finally, the third part consists in understanding the preferred oxidant to attack ibuprofen and the most likely sites of interaction between the radical and the ibuprofen molecule using a simple computational calculation through DFT theory.

2 Materials and methods

2.1 Photocatalytic tests

Commercial TiO_2 solid was used for all tests (Vetec, 98% of purity and average particle size of 100 nm). The photocatalytic reaction was performed at room temperature and atmospheric pressure. The process was made by irradiating a mercury lamp (125 W) through the ibuprofen solution. The wooden photocatalytic system was internally covered with aluminum foils to make better use of all radiation emitted. The mixture was kept in the dark for 30 min to establish the adsorption–desorption equilibrium of the solution before light irradiation. The first degradation test was performed using only the light effect without the catalyst using 100 mL of ibuprofen 10^{-4} M with an initial pH = 7. Then, the different variables were evaluated using titanium dioxide. Three different masses of TiO_2 were analyzed in the following proportions 0.1, 0.3, and 0.5 g of photocatalyst per liter of ibuprofen solution. Afterwards, in order to evaluate the pH effect on the photodegradation, tests with 100 mL of ibuprofen solution and 0.03 g of TiO_2 using pH of 3.0, 6.0, and 9.0 were carried out.

The photodegradation reaction was followed by UV-VIS characterization using a UV-VIS Spectrophotometer Shimadzu 1800. The

absorbance from 200 to 350 nm was measured. For this analysis, aliquots of 3 mL were collected at predetermined times. The aliquots were collected with a syringe using a hose from solution to the external part of the photoreactor. Filters of 0.20 μm were used to filter the ibuprofen solution with TiO_2 from each collected aliquot. The degradation rate was calculated according to eqn (1).

$$\text{Degradation rate}(\%) = \frac{C_0 - C_t}{C_0} \times 100\% \quad (1)$$

2.2 Photocatalyst characterization

The X-ray diffraction analysis (XRD) were made by using a Bruker D2 Phaser Diffractometer with CuKα ($\lambda = 1.54$ Å) radiation. The analysis was taken at a 2θ angle between 10 and 90°. The phase identification was made by using X-Pert HighScore Panalytical software and database JCPDS-ICDD 2003.[29,30] Rietveld refinement was performed by operating MAUD and GSAS software[31] using EXPGUI interface,[32] after determining instrumental widening through the refinement of LaB_6 standard sample. The modified Pseudo-Voigt function (Thompson–Cox–Hastings) was chosen to adjust the diffraction peaks profiles of the identified crystalline phases.[33]

For TiO_2 band-gap energy determination, it was used a UV-Vis-NIR Agilent Cary 5000 Spectrophotometer, which is equipped with a 150 mm diameter integration sphere on the external reflectance accessory (DRA-2500). The reflectance signals were obtained in a wavelength range from 200 to 900 nm. To find the band-gap energy, it was used the Tauc model for indirect transitions. Eqn (2) was used for the transition conversions. This model is represented by the curve of energy quantities *hv versus* the quantities $(\alpha hn)^{1/n}$. The band-gap energy is determined from the extrapolation of the straight line to the abscissa axis (hv).[34]

$$(\alpha hv)^{1/n} = \beta(hv - E_g) \quad (2)$$

where α is the material absorption coefficient, h and v are respectively, plank constant and the light frequency, n is relative to transition nature ($n = 2$ for indirect allowed transitions and $n = 1/2$ for direct allowed transitions), β is parameter constant from each band tail, and E_g is the band-gap optical energy. Normally, to obtain the band-gap energy by the Tauc method, it is necessary to obtain the absorbance and transmittance from spectra, however, as it was used the reflectance results, it was necessary to readapt, by using the Kubelka–Munk model, shown in eqn (3).

$$[F(R\infty)hv]^{1/n} = A(hv - E_g) \quad (3)$$

where the expression $F(R\infty)$ is a Kubelka–Munk function, proportional to absorption coefficient α, and A is the absorption parameter. To determine the $F(R\infty)$ value, it was used eqn (4), where R is the reflectance values.

$$F(R) = \frac{(1-R)^2}{2R} \quad (4)$$

The Tauc model was adapted and it was plotted the spectra of $[F(R\infty)hv]^{1/n}$ *versus* hv, consequently, the band-gap energy was found by extrapolating the line in $F(R) = 0$.

The N_2 adsorption–desorption isotherm was performed at 77 K using a Micrometrics sortometer equipment, model ASAP 2020, with a turbomolecular pump. The sample was previously degassed at 200 °C for 2 h. The specific surface area (S_{BET}) was obtained by Brunauer, Emmet and Teller (BET) method,[35] using the adsorption data and taking into account the IUPAC recommendations.[36] The total pore volume (V_p) was obtained by the Gurvich rule.[37]

The zeta potential analysis was performed using a Stabino particle charge titration analyzer (Colloid metrix), adjusting the pH along the measurements. This equipment uses an oscillating piston design. It is necessary to use a cylindrical PTFE chamber with an oscillating piston, both carrying anionic charge at the surface. A fraction of the particles was immobilized at the surface. Thus, the mobile cloud was pushed up and down with the piston movement. The oscillating ion cloud generated an alternating voltage at the electrodes, which is related to the zeta potential. 40 μL of a NaOH solution was added every 15 s until the pH is 12.0, and HCl solution was added until the pH is 2.0. The created potential is detected and measured by the two electrodes, enabling a zeta potential plot to be obtained as a function of pH. The isoelectric potential of the solid was determined from this curve.

Gas chromatography-mass spectrometry (GC-MS) were performed to identify the by-products formed from the photocatalytic degradation of ibuprofen, model GC-2010 Plus from Shimadzu, with polar column (30 m × 0.25 mm × 0.25 μm) and automatic injection model AOC-20i. The photocatalyst was separated from the ibuprofen solution using filters 0.20 μm after 5 min of photodegradation. Then, the solutions were treated with a ethanol : ibuprofen ratio of 2 : 1 and 1 μL (split less) was injected. A heating ramp from 100 °C to 270 °C with a heating rate of 15 °C min^{-1} was used. The injector temperature was 270 °C. The NIST library (National Institute of Standards and Technology) was used to identify the by-products.

A model reaction using salicylic acid as probe molecule was performed and accompanied by UV Vis spectroscopy analysis to assess the presence of the hydroxyl radical. A photocatalytic reaction was performed using a 5.0×10^{-4} M solution of salicylic acid applying a similar methodology to photocatalytic tests. The same catalyst was used, in the proportion of 0.3 g per liter of solution, the same irradiation source, the same aliquot volume and the same filter. Aliquots were withdrawn at intervals of 5, 15, 30 and 60 min. The photoreaction was followed by UV-VIS spectroscopy in the range of 250–400 nm using the Shimadzu 1800 UV-VIS Spectrophotometer.

2.3 Theoretical-computational calculation (DFT approach)

All optimization and energy calculations were obtained using a DFT approach in gas phase through the B3LYP,[38] B3LYP-D3,[39] cam-B3LYP,[40] B3P86,[41] wB97X-d,[42] MN12-L,[43] MN12sx,[44] PBE,[45] PBE0 (ref. 46 and 47) and TPSSH[48] methods with the 6-31G(d, p) base set[49] in order to evaluate the ibuprofen experimental infrared spectra data and predict the best model that describes the structure. The error calculation was obtained from the sum of theoretical wavelengths minus the sum of the experimental wavelength divided by the sum of experimental wavelengths,[50] according to eqn (5).

$$\text{Error } (\%) = \frac{\sum(\text{theoretical wavelength}) - \sum(\text{experimental wavelength})}{\sum(\text{experimental wavelength})} 100\% \quad (5)$$

It was determined the molecular electrostatic potential map for ibuprofen in gas phase to observe the regions of greater electronic density. Furthermore, the DFT method that obtained the smallest deviation from the experimental data was the method chosen to study the spontaneity of the ibuprofen reaction interacting with $OH^{\bullet}$ radical in seven different positions in gas phase using the free energy of each position. The calculations in the same seven positions were also performed taking into account the solvent (water) using the polarized continuum model (PCM). All calculations were performed using Gaussian 09 software.[51]

3 Results and discussion

3.1 X-ray diffraction (XRD)

Titanium dioxide may have three possible crystalline phases, anatase, rutile and brookite, depending on the synthetic conditions employed. XRD was used to identify which of these phases were present in the photocatalyst. The diffractogram is presented in Fig. S1a.†

The presence of the anatase and rutile phases was observed. The first phase related to anatase can be identified with 2θ peaks values of 25.22°, 37.76°, 47.90°, 53.96°, and 54.98°, which Miller indices (*hkl*) are (101), (004), (200), (105), and (211), respectively. The second phase concerning the rutile can be identified by 2θ peaks values of 27.42°, 35.99°, 41.21°, and 56.58° with Miller indices Miller (*hkl*) (110), (101), (111), and (220), respectively.

In order to quantify each phase observed, a refinement was performed from diffractogram using Rietveld method. The results are presented in Fig. S1b.† It was observed that sample has 84.85% of TiO_2 in the anatase phase and 15.15% in rutile structure. The higher quantity of the anatase phase compared to rutile is very interesting for photocatalysis applications, since this phase has better photocatalytic properties due to its smaller recombination of electron–hole pair.[15]

3.2 Band-gap energy

The curve related to $[F(R\infty)h\nu]^{1/n}$ *versus* hν spectra is shown in Fig. S1c.† It was determined the band gap energy using the Tauc model adapted by the Kubelka–Munk model. In this case, it was considered $n = 1/2$ for indirect allowed transition, which, according to the literature, is predominantly titanium dioxide.[34] The TiO_2 band gap energy obtained by the extrapolation of the line was 3.29 eV as expected, which is in accordance with previously described values for rutile and anatase phases.[52]

3.3 Textural properties

N_2 adsorption/desorption analysis was performed to investigate the textural properties of TiO_2 oxide. The result is shown in Fig. S1d.† A non-significant hysteresis curve, a type III isotherm with S_{BET} area of 8 $m^2\ g^{-1}$ and pore volume (V_p) of 0.02 $cm^3\ g^{-1}$ were observed. Type III isotherm is related to non-porous or macroporous solids. Low surface area values are typical of pure titanium oxide.[53] Considering that TiO_2 has low porosity, the V_p value is certainly due to the interaction between particles.

3.4 Thermal stability study

In order to evaluate the impact of the temperature in the ibuprofen degradation, a 10^{-4} M solution was heated at temperatures of 30, 40, 50 and 60 °C. The results of the wavelength and absorbance are exhibited in Fig. S2.†

The band used for ibuprofen thermal stability evaluation is at approximately 220 nm. One can notice that this band did not have any change with the temperature increase up to 60 °C. Considering that in the photocatalytic medium used in this work there is a temperature increase of 5 °C in relation to the room temperature, the temperature effect cannot lead to the ibuprofen degradation. Therefore, the photocatalysis results discussed, are caused exclusively by the light effect with or without the catalyst and it was not affected by the temperature.

3.5 Effect of mass on photodegradation

The degradation was accompanied by a decrease in the ibuprofen band at 222 nm according to the UV-Vis absorption spectra results. It is essential to mention that this decrease does not necessarily mean that the drug has been totally mineralized, since it may be converted in other molecules as well, generating different by-products. To prevent adsorption effects in photocatalytic tests, before starting each reaction, the solution-catalyst mixtures were stirred in the dark, until equilibrium was reached. Similar adsorption capacities were observed for all cases, with an average of 3.8%. The low adsorption capacity demonstrates that this step does not significantly interfere in the results of photocatalytic reactions.

The Fig. S3† shows the maximum absorbance for each band and the time of radiation exposure. The spectra related to the wavelength *versus* absorbance are in the ESI.† One can notice in Fig. 1a that the absorbance decrease is faster when one increases the catalyst mass. The degradation kinetics presented the following increasing order <0.01 g of TiO_2 <0.03 g of TiO_2 <0.05 g of TiO_2. This observation can also be made by analyzing the degradation rate shown in Fig. 1b.

Fig. 1b confirms the efficiency of titanium dioxide for ibuprofen degradation reaction. It was verified that the reactions using 0.01 g of photocatalyst reach 100% of degradation in 30 min, while the reaction with 0.05 g of TiO_2 was the fastest solid, which it was necessary only 10 minutes to achieve maximum degradation, corroborating with the positive effect of

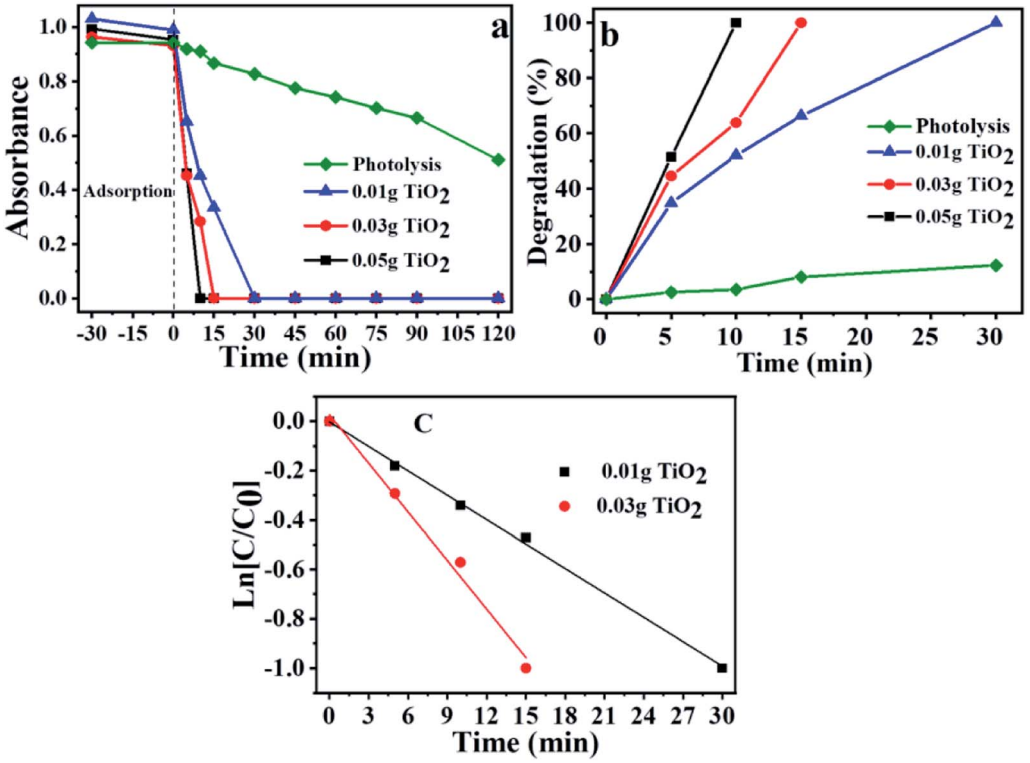

Fig. 1 (a) Influence of different photocatalyst masses on ibuprofen degradation; (b) ibuprofen (10^{-4} M) degradation rate *versus* irradiation time for the different masses; (c) pseudo-first order reaction for ibuprofen degradation.

the mass increase in the degradation time. In the photolysis without the presence of photocatalyst, 30 min are needed to obtain only 12.40% of the degradation, and for the time of 120 min, 46.43% of degradation was observed, demonstrating that the light effect alone is not enough to degrade ibuprofen and the presence of the TiO_2 is essential to complete drug degradation.

The ibuprofen degradation reaction follows a pseudo-first-order kinetics (Fig. 1c), which is in agreement with previously published studies.[54–56] Thus, it is possible to calculate the pseudo-first kinetic constant (K') and the half-life times ($T_{1/2}$) for each reaction using eqn (6) and (7), and plotting the graph of ln $[C/C_0]$ *versus* time (Fig. 1c) based on eqn (7), where k is the slope of the generated line and C is the concentration in each time, C_0 is the initial concentration and t is the time. The half-life for each reaction was also calculated using the eqn (7).

$$\ln\left[\frac{C}{C_0}\right] = -kt \quad (6)$$

$$t_{1/2} = \frac{\ln 2}{k} \quad (7)$$

Table S1† shows the correlation coefficient (R^2), the pseudo-first rate constant (k'), and the half-life time ($t_{1/2}$). It is possible to notice that the reaction occurs faster when one increases the catalyst mass. The presented values indicated that for the greater the TiO_2 mass used, it was obtained a higher rate constant and a smaller half-life time. Greater mass of solid used, greater is the number of active sites, and consequently, photocatalytic activity is higher.

3.6 pH influence on photocatalytic activity

The pH can directly influence the photocatalytic degradation according to previously published works.[57,58] To analyze the pH effect on the photoreactions, it was used for all cases the following parameter: 0.03 g of TiO_2 in 100 mL of 10^{-4} M ibuprofen solution. The pH was controlled by HCl (0.01 M), and NaOH (0.01 M) solutions. Fig. 2 shows the photodegradation behavior of ibuprofen using a pH of 3.0, 5.0, 7.0 and 9.0, respectively.

The reaction at pH 5.0 presented the best photocatalytic performance, which the disappearance of band at 222 nm was observed within 5 min, reaching 100% degradation. This behavior can be explained by correlating the surface charge of the catalyst with the predominant charge in the solution. The surface charge of the catalyst depends on the chemical nature and the pH, which is related to the point of zero charge (pHpzc).[58] For pH values below the pHpzc, the catalyst particles are protonated and are positively charged, while pH above pHpzc, the catalyst is deprotonated and are negatively charged.

The pHpzc is between 3.8 and 6.5 for TiO_2, depending on the particles size according to previous study.[57,58] Ibuprofen is a weak acid with a pK_a of 4.91. At a pH value below the pK_a, ibuprofen molecule is protonated, while at a pH above pK_a, ibuprofen is in its anionic form.[57] Thus, situations in which the pH is lower than the pK_a or higher than the pHpzc, both catalyst

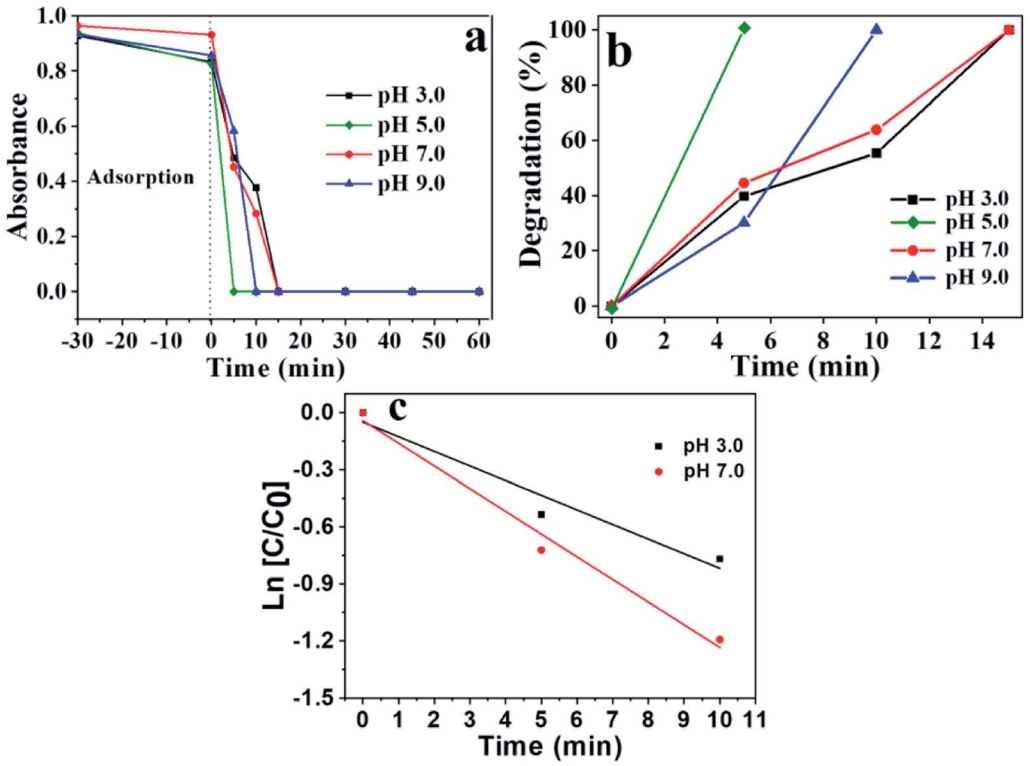

Fig. 2 (a) Influence of pH on ibuprofen photodegradation; (b) ibuprofen (10^{-4} M) degradation rate *versus* irradiation time for the different pHs; (c) pseudo-first order reaction for ibuprofen degradation.

and ibuprofen will have positive and negative charge, respectively, promoting an electrostatic repulsion between them, which may cause a decrease in its photodegradation power. This behavior can be seen in Fig. 2 for pH 3.0 and 7.0. On the other hand, the medium at pH 5.0 is within a range where the pH is higher than pK_a and lower than pHpzc, therefore, the solution is in anionic form and the photocatalyst is positively charged, causing an electrostatic attraction, which contributes to better adsorption of the ibuprofen molecule on the TiO_2 surface, favoring a greater degradation performance. For this pH, it was observed the best photocatalytic result.

However, the results for pH = 9 do not follow the justification presented above, since it was expected smaller performance compared to pH = 7.0. An explanation proposal for greater efficiency is due to the larger amount of OH^- present in the medium that can provide increased production of hydroxyl radicals, main responsible species for the photodegradation, compensating the electrostatic repulsion. The highest efficiency in alkaline medium was found for photolysis at different pH according to previously results.[56]

Zeta potential analysis was carried out in order to confirm the information described above. The result is shown in Fig. 3. The point where the surface charge density is equal to zero is designated as point of zero charge (PZC),[57,58] while the point where the zeta potential is equal to zero is named isoelectric point (IEP) and the catalyst surface is neutral on these points.[59]

If there is no interference from specific adsorption on the catalyst surface, the PZC and IEP present the same result.[59,60] It is known that the TiO_2 particle show negative surface charge or zeta potential when pH values are higher than pH_{IEP}, while for pH lower than pH_{IEP} the charge on the titanium dioxide surface is positive,[57,58] as seen in Fig. 3.

The isoelectric point was found at pH = 5.2. This obtained value corroborates with the degradation results presented in Fig. 2, which the best results were observed at pH = 5.0. In this case, the pH of the medium is below the pH_{IEP} of TiO_2 and higher than the pK_a of ibuprofen (4.85), consequently, the catalyst surface has negative charges while ibuprofen is positively charged, generating an electrostatic attraction, which contributes to greater drug adsorption on the photocatalyst surface, increasing the efficiency in photodegradation. The interaction between the charges of titanium dioxide and

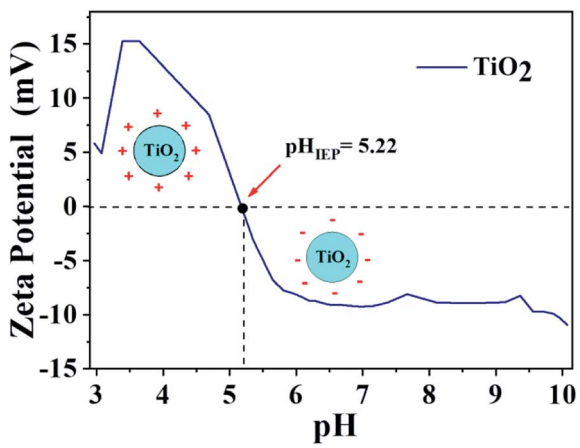

Fig. 3 Zeta potential for TiO_2 photocatalyst.

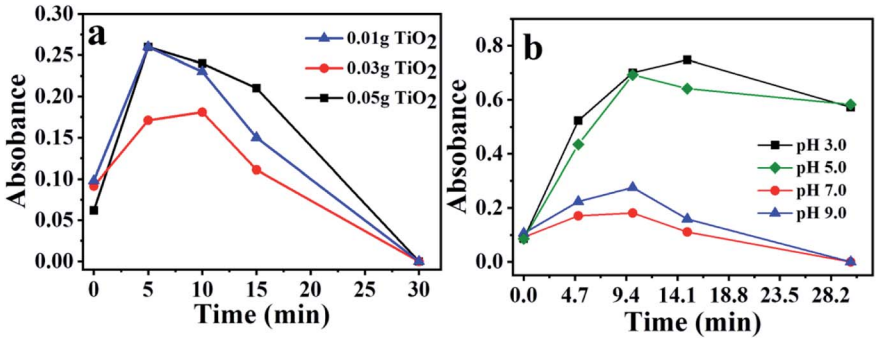

Fig. 4 (a) By-product formation *versus* irradiation time for the different masses used; (b) influence of pH on by-products formation.

ibuprofen for different pH ranges is presented in Scheme S1,† illustrating the regions of attraction and repulsion depending on the pH range, charges of ibuprofen and TiO_2. The adsorption capacity for the process in the absence of light was also evaluated for reactions at different pHs, Fig. 2a. The average adsorption capacity for the different pHs was 8.3%. The highest adsorption capacity was observed at pH 5, reaching values of 11.7%, corroborating the zeta potential results. The low adsorption capacity once again demonstrates that this step does not significantly influence the photocatalysis results.

Fig. 2c confirms that the ibuprofen degradation reaction follows a pseudo-first order kinetics due to the linear behavior of the graph $\ln[C/C_0]$ against time, corroborating previous studies.[54–56] Table S2† shows the values of correlation coefficient (R^2), half-life ($t_{1/2}$), pseudo-order rate constant (k'), varying the pH. The values showed that besides the mass effect, pH also affects the kinetic parameters obtained. The reaction at pH = 7 showed a higher degradation rate compared to pH = 3, which are in accordance with the degradation results present in Fig. 2b.

The TiO_2 photocatalyst activity was compared with other previously published works which studied the ibuprofen degradation, taking into account the different reaction conditions used.[18,61–67] The different results are shown in Table S3.† It is observed that the present study indicated high performance and, mainly, shorter time for complete ibuprofen degradation compared to other similar solids, which is related to the low band gap energy and the small particle size.

3.7 Effect of the mass and pH on the by-product formation

The UV spectra are present in Fig. S4† for the different reaction times varying the pH, supplementary material. One can noticed the presence of a new band around 225 nm in which the intensity increases over time, while the band at 222 nm concerning the ibuprofen decreases. This characterizes an appearance of by-products from the oxidation of the organic molecule, indicating that, initially, the ibuprofen degradation is not promoting the complete mineralization, but producing intermediate species. This behavior can be seen in Fig. 4a and b.

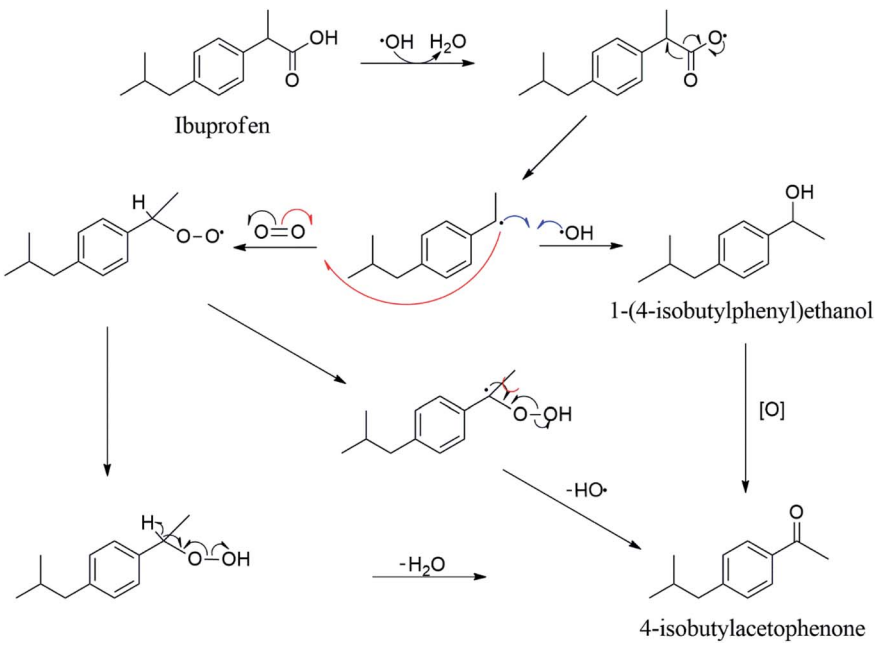

Scheme 1 Proposal formation of by-products through ibuprofen photodegradation.

Fig. 4a is related to the band increases at 225 nm for the different masses, showing the formation of by-products. It is noted that, for the smallest and largest mass of TiO_2, the results are similar; however, for an intermediate amount of catalyst using 0.03 g, the band increase is less significant. Another interesting aspect observed in Fig. 4a, is related to the fact that in 30 min of reaction, the band at 225 nm disappears for the three masses. This may be an indication that after this period, the mineralization process is more pronounced.

Fig. 4b shows a discrepancy among the absorbance values obtained for the different pHs studied. In acidic pH, there is a tendency to form higher quantities of by-products, while in neutral or in alkali pH is less pronounced. Cory *et al.* proposes that the by-product responsible for the appearance of the band at 255 nm is 4-isobutylacetophenone.[67] The process occurs through decarboxylation reaction followed by oxidation. Other works[58–60] showed the mass spectra for ibuprofen degradation, which it was possible to identify the presence of 4-isobutylacetophenone among all the degradation products. It is shown in Scheme 1 the possible reaction pathways for the ibuprofen conversion to 4-isobutylacetophenone. In this case, the reactions involving the formation of hydroxyl radical in the presence of oxygen.

The by-product formed may be influenced by pH, which is more favorable in an acid medium, corroborating with the observations presented in Fig. 4b. In addition, it can be seen that the absorbance band at 255 nm disappears in 30 min of reaction, indicating that ibuprofen was totally degraded. However, the degradation rate may be superior at pH 7.0 or 9.0, since in 30 min of reaction there are not observable bands, while for lower pH the by-product band at 255 nm remains present.

A sequence of reactions was described to understand the degradation pathway of ibuprofen in the presence of the titanium-based photocatalyst. Reaction (8) refers to the beginning of the reaction process, which the formation of electron–hole pair occurs caused by the action of irradiation, light. Subsequently, reactions (9)–(12) show the interaction of the contaminant with the catalyst surface forming three possible radicals due to the breakdown of the initial molecule (IBU*, IBU**, IBU***). As previously reported,[56,57] a band with a maximum value around 255 nm increases the intensity during the degradation of ibuprofen with UV irradiation according to the ultraviolet (UV)-visible spectroscopy results, which has been related to the generation of by-products such as decarboxylated, hydroxylated, dihydroxylated and demethylated species[68] and justifies the formation of radicals. Among the main by-products formed, 4-isobutylacetophenone has shown prominence according to the reaction sequence described in Scheme 1. The main by-products identified are present in Table 1 and Fig. S5† according to the GC-MS results, confirming the formation of species 4-isobutylacetophenone, *p*-isobutylbenzaldehyde, 4-methyl-2-phenyl-1-penten-3-ol, 4-phenyl-benzylacetone and 3-phenyl-2-butanone.

Reaction (12) shows the capture of electrons by the oxygen present in the medium, forming superoxide radicals. The superoxide radicals formed react with the acid medium to form another radical species ($HO_2^{\bullet}$), reaction (13). Reaction (14) describes the dimerization of the hydroperoxide radical, forming the hydrogen peroxide molecule, which decomposes into $OH^{\bullet}$ and OH^- species according to reaction (15). In addition, reaction (16) demonstrates the attack of the hydroxyl radical on activated ibuprofen species to drive their complete degradation.

Table 1 By-products identified during the photocatalytic degradation of ibuprofen by GC-MS

By-products	Molecular weight (g mol^{-1})	Structure	% similarity with NIST	Major ions
Ibuprofen	206	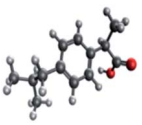	94	41, 77, 91, 119, 145, 161, 191, 206
4-Isobutylacetophenone	176	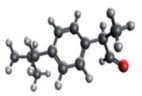	91	43, 77, 91, 119, 134, 161, 178
3-Phenyl-2-butanone	148	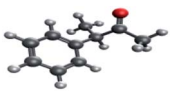	77	43, 77, 105, 106, 148
p-Isobutylbenzaldehyde	162	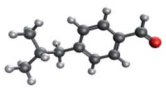	72	43, 65, 91, 120, 136, 162
4-Phenyl-benzylacetone	148	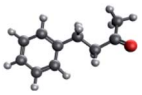	80	43, 77, 105, 106, 148
4-Methyl-2-phenyl-1-penten-3-ol	176	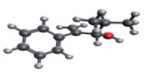	81	43, 77, 105, 106, 133, 176

Reaction (17) describes the neutralization of acid-base species. Finally, reaction (18) represents the global process by eliminating several species represented in reactions between 1 and 10, consequently, obtaining CO_2 and H_2O as products, leading to the mineralization of the organic pollutant.

Surface steps

$$3h\nu + 3TiO_2 \rightarrow 3h^+ + 3e^- \quad (8)$$

$$h^+ + IBU \rightarrow IBU^* + H^+ \quad (9)$$

$$h^+ + IBU \rightarrow IBU^{**} + H^+ \quad (10)$$

$$h^+ + IBU \rightarrow IBU^{***} + H^+ \quad (11)$$

Solution steps

$$2e^- + 2O_2 \rightarrow 2O_2^{-\bullet} \quad (12)$$

$$2O_2^{-\bullet} + 2H^+ \rightarrow 2HO_2^{\bullet} \quad (13)$$

$$HO_2^{\bullet} + HO_2^{\bullet} \rightarrow O_2 + H_2O_2 \quad (14)$$

$$H_2O_2 + e^- \rightarrow OH^{\bullet} + OH^- \quad (15)$$

$$IBU^* + IBU^{**} + IBU^{***} + 2OH^{\bullet} \rightarrow H_2O + CO_2 \quad (16)$$

Acid and base reaction (neutralization)

$$OH^- + H^+ \rightarrow H_2O \quad (17)$$

Global reaction

$$3IBU + 2O_2 + 3h\nu \rightarrow H_2O + CO_2 \quad (18)$$

In order to complement the described reaction sequence, a possible reaction pathway for the photocatalytic oxidation of ibuprofen is shown in Scheme 2, indicating the different oxidants radicals possible to degrade ibuprofen. Initially, the incidence of radiation on the titanium dioxide-based surface leads to the creation of electrons and holes represented by e^- and h^+, respectively, already described in reaction (8), which react with water on the surface and generate strong oxidants species ($HO_2^{\bullet}$, $O_2^{-\bullet}$ and $OH^{\bullet}$) and it can also react with the contaminant forming various by-products, as represented in reactions (9)–(11), respectively. It is worth mentioning again that the by-products formed were identified by GC-MS according to Table 1 and Fig. S5.† The oxygen molecules react with the photogenerated electron to form the peroxyl radical ($O_2^{-\bullet}$), reaction (12), which can react with H^+ forming the hydroperoxide radical ($HO_2^{\bullet}$), reaction (13), or it can directly attack by-products from the ibuprofen degradation. On the photocatalyst surface, water molecules react with positive vacancies to generate $OH^{\bullet}$ radicals. In this step, the solid surface abstracts an electron and, consequently, the regeneration of the active phase occurs. The regeneration of the solid was confirmed by XRD analysis after photoreaction, which showed a similar XRD profile before the reaction, Fig. S6.† Finally, the photogenerated radicals ($O_2^{-\bullet}$, $HO_2^{\bullet}$, $OH^{\bullet}$) with high oxidation capacity are able to oxidize the pollutant molecule and its by-products into lighter compounds and most of these light compounds undergo more oxidation reactions and are eventually converted to CO_2 and water, thus, they are mineralized.

As already presented in Scheme 2 and described in the different elementary steps of the mechanism, the three possible radicals capable of degrading the ibuprofen molecule are hydroperoxyl ($HO_2^{\bullet}$), peroxyl ($O_2^{-\bullet}$) and hydroxyl radical ($OH^{\bullet}$). It is worth mentioning that the formation of these radicals is triggered by the formation of the electron–hole pair. The hydroxyl radical, with a one-electron reduction potential of +2.33 V, is a powerful oxidant reacting with organic species such as ibuprofen compared to hydroperoxyl (−0.88 V) and peroxyl radical (−2.40 V).[69,70]

Salicylic acid can be used as a probe molecule to experimentally identify the presence of hydroxyl radical.[71–75] The model reaction between salicylic acid and $OH^{\bullet}$ radical forms two primary products, designated as 2,3-dihydroxybenzoic acid

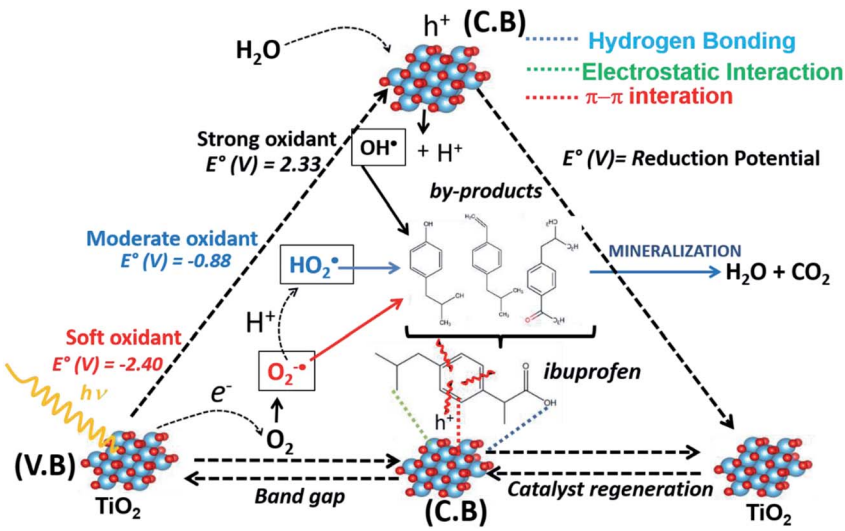

Scheme 2 Illustrative mechanism for the photodegradation reaction of ibuprofen using TiO_2-based catalyst.

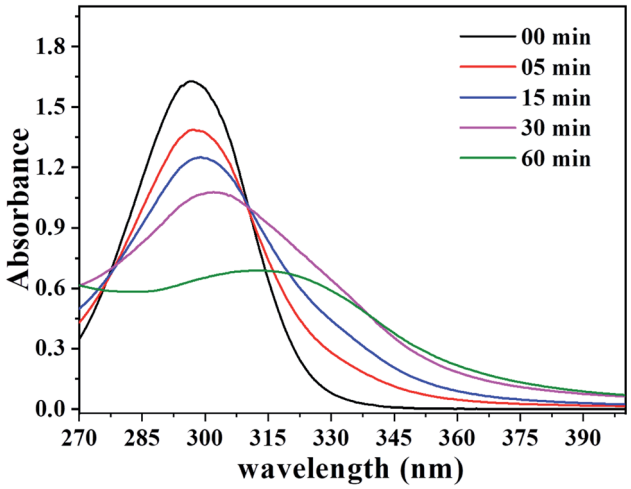

Fig. 5 UV-Vis spectra referring to the photoreaction of salicylic acid with the OH$^{\bullet}$ radical catalyzed by TiO_2.

and 2,5-dihydroxybenzoic acid, shown in Fig. S7.† This reaction can be observed using UV-Vis spectroscopy.[75] Fig. 5 shows the UV-Vis spectra for the photocatalytic reaction of salicylic acid in the presence of TiO_2. Initially, it is possible to observe the salicylic acid spectra with a characteristic band at approximately 300 nm. After starting the reaction, a change is noted in two regions of the spectra. The decrease in the intensity of the salicylic acid band can be seen related to the decrease in its concentration. Furthermore, there are a small shifts in this band to longer wavelengths, as well as the increase in absorbance intensity in the region between 320 and 400 nm during the reaction time. According to previous studies,[47] these changes characterize the presence and increased concentration of 2,3-dihydroxybenzoic acid and 2,5-dihydroxybenzoic acid products, therefore, it is possible to confirm the production of hydroxyl radicals by irradiating UV light on the TiO_2 surface in solution.

A simple theoretical-computational study was carried out in order to determine the preferred positions of attack by OH$^{\bullet}$ radical in the ibuprofen molecule. The results presented after

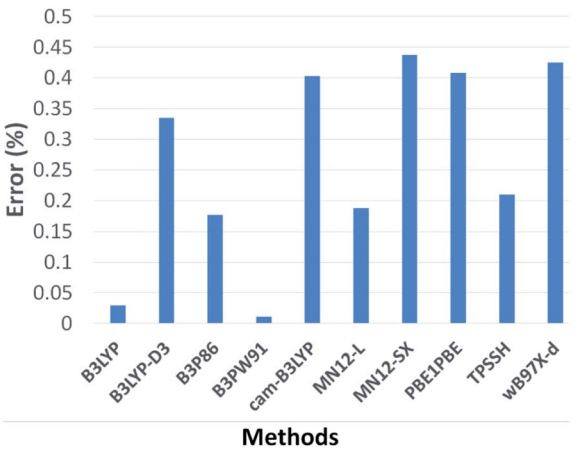

Fig. 6 Optimization and error calculations of the ibuprofen structure using different methods.

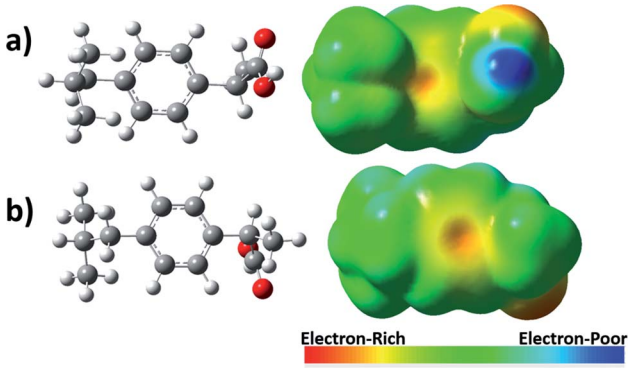

Fig. 7 Map of electrostatic potential for ibuprofen in two different positions showing carboxyl groups in the (a) front and (b) back views. The color scale indicates the electron rich and poor regions.

calculations of the chosen DFT methods designated as B3LYP, B3LYP-d3, B3P86, B3PW91, CAM-B3LYP, MN121, MN12SX, PBELPBE, TPSSH, WB97X-D are represented in Fig. 6. Computational data were compared with ibuprofen wavenumbers of 864, 937, 1074, 1178, 1228, 1327 and 1419 cm^{-1} extracted from FTIR experimental results[50] in order to obtain an efficient simulation approach.

It is observed that all the highlighted methods have an approximation above 99% based on the chosen experimental parameters, enabling a large number of acceptable alternatives for calculations. However, the B3PW91 method showed a smaller deviation from the experimental data, thus, it was the method chosen to perform all calculations.

In addition, for a better understanding of the interaction between ibuprofen and oxidants radicals, an analysis of the density-to-potential map for the ibuprofen was performed and their possible chemical bonding points were observed, Fig. 7. It was visualized in the density map based on the electrostatic potential that the regions with the highest electron density are in red around oxygen and with a slight yellow color around the carbon–carbon double bond from aromatic ring. It is important to mention that free radicals such as OH$^{\bullet}$ prefer to attack regions with higher electron density, which is located around the aromatic ring.

Afterward, it was analyzed seven different interaction positions between the OH$^{\bullet}$ radical and ibuprofen in gas phase, specifically in the sites where a higher electron density was observed according to the electrostatic potential map (Fig. 7). Gibbs free energy was obtained for each position. The obtained results are shown in Fig. 8. The results of free energy extracted were −101.27, −101.37, −101.74 and −102.16 kcal mol^{-1} for the positions 1, 2, 3 and 4, respectively, concerning the interaction of the hydroxyl radical with the aromatic ring. The values were quite similar in the four different positions; however, it was possible to infer that position 4 presented the most favorable energy due to the lowest value of free energy and, therefore, it is characterized as the most thermodynamically favorable interaction. On the other hand, the results of free energy in positions 5, 6 and 7 were −42.69, −93.44 and −92.48 kcal mol^{-1}, respectively. The interaction of hydroxyl radicals with the

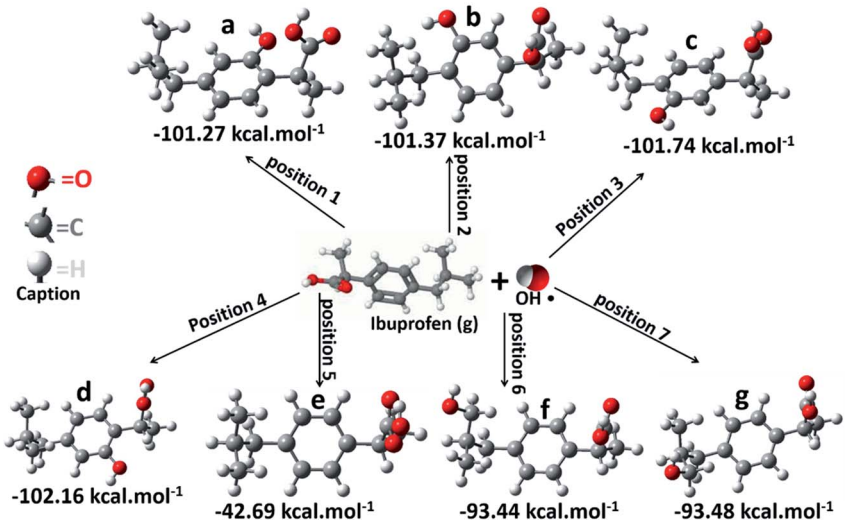

Fig. 8 Schematic representation of ibuprofen/•OH radical system in gas phase after optimization used to calculate free energy for the seven different positions.

carboxyl groups present in the ibuprofen molecule (position 5) is less thermodynamically favorable compared to other positions, showing the highest value of free energy. Thus, the hydroxyl radicals can effectively break double bonds (C=C), degrade hydrocarbons and ring opening of aromatics due to electrophilic nature of OH•, consequently, can promote the degradation and mineralization of ibuprofen, corroborating the sequence of elementary reactions and Scheme 2 described above.

Similar calculations were performed taking into account the presence of the solvent, water. The results are shown in Fig. S8.† The same spontaneity order was observed, in which position 4 was the most favorable, confirming that the OH• radical preferentially attacks the aromatic ring. The small difference in free energy values is due to the presence of water.

4 Conclusion

Insights into the mechanism for degradation of ibuprofen, mentioning the formation of by-products, were presented and aspects related to the preferential attack by oxidants radicals in different sites of the ibuprofen molecule were also mentioned based on experimental and simple theoretical-computational results. It was observed the presence of the anatase (84.4%) and rutile (15.6%) phases with the band-gap energy value of 3.29 eV for the photocatalyst used in all tests.

Photoreaction was favored at pH 5.0 due to the electrostatic attraction between TiO_2 and ibuprofen, considering that in this pH range the species have opposite charges. The concentration of by-products formed depends on the reaction conditions such as pH and a high degradation rate referring to the reduction of the ibuprofen absorption band does not necessarily mean a high mineralization rate, which depend on the intensity of the bands related to the by-products. The different by-products formed were identified by GC-MS, which can highlight presence of 4-isobutylacetophenone.

The degradation and mineralization of ibuprofen follows a sequence of elementary reactions in solution and on the surface, producing a series of oxidants radicals such as $O_2^{-\bullet}$, $HO_2^{\bullet}$ and OH• capable of degrading the organic matrix. The simple computational theoretical study showed that OH• radicals preferentially attack the region with the highest electronic density of the ibuprofen molecule located around the aromatic ring close to the C=C bonds, which is related to electrophilic character of OH•. The presence of OH• was experimentally confirmed by measuring hydroxyl radicals using salicylic acid as probe molecule.

Conflicts of interest

There are no conflicts to declare.

Acknowledgements

The authors would like to thank the Brazilian CNPq and CAPES funding agencies for financial support. Professor Marco A. Morales Torres of Federal University of Rio Grande do Norte for helping with the XRD analysis.

References

1 V. Geissen, H. Mol, E. Klumpp, G. Umlauf, M. Nadal, M. van der Ploeg, S. E. A. T. M. van de Zee and C. J. Ritsema, Emerging pollutants in the environment: A challenge for water resource management, *Int. Soil Water Conserv. Res.*, 2015, **3**, 57–65, DOI: 10.1016/j.iswcr.2015.03.002.
2 T. Deblonde, C. Cossu-Leguille and P. Hartemann, Emerging pollutants in wastewater: A review of the literature, *Int. J. Hyg. Environ. Health.*, 2011, **214**, 442–448, DOI: 10.1016/j.ijheh.2011.08.002.
3 M. la Farré, S. Pérez, L. Kantiani and D. Barceló, Fate and toxicity of emerging pollutants, their metabolites and

transformation products in the aquatic environment, *TrAC, Trends Anal. Chem.*, 2008, **27**, 991–1007, DOI: 10.1016/j.trac.2008.09.010.

4 D. M. Bila and M. Dezotti, Fármacos no meio ambiente, *Quim. Nova*, 2003, **26**, 523–530, DOI: 10.1590/s0100-40422003000400015.

5 R. López-Serna, M. Petrović and D. Barceló, Occurrence and distribution of multi-class pharmaceuticals and their active metabolites and transformation products in the Ebro River basin (NE Spain), *Sci. Total Environ.*, 2012, **440**, 280–289, DOI: 10.1016/j.scitotenv.2012.06.027.

6 F. De Logu, S. Li Puma, L. Landini, T. Tuccinardi, G. Poli, D. Preti, G. De Siena, R. Patacchini, M. G. Tsagareli, P. Geppetti and R. Nassini, The acyl-glucuronide metabolite of ibuprofen has analgesic and anti-inflammatory effects *via* the TRPA1 channel, *Pharmacol. Res.*, 2019, **142**, 127–139, DOI: 10.1016/j.phrs.2019.02.019.

7 K. Gurung, M. C. Ncibi, S. K. Thangaraj, J. Jänis, M. Seyedsalehi and M. Sillanpää, Removal of pharmaceutically active compounds (PhACs) from real membrane bioreactor (MBR) effluents by photocatalytic degradation using composite Ag_2O/P-25 photocatalyst, *Sep. Purif. Technol.*, 2019, DOI: 10.1016/j.seppur.2018.12.069.

8 Y. Wang, S. Zhan, Y. Ge, C. Wang, J. Hu and H. Liu, Highly efficient photocatalytic degradation of tetracycline using a bimetallic oxide/carbon photocatalyst, *Acta Phys.-Chim. Sin.*, 2020, **36**(8), DOI: 10.3866/PKU.WHXB201905083.

9 X. Du, X. Yi, P. Wang, J. Deng and C. C. Wang, Enhanced photocatalytic Cr (VI) reduction and diclofenac sodium degradation under simulated sunlight irradiation over MIL-100 (Fe)/g-C_3N_4 heterojunctions, *Chin. J. Catal.*, 2019, **40**(1), 70–79, DOI: 10.1016/S1872-2067(18)63160-2.

10 Q. Y. Tang, R. Huo, L. Y. Ou, X. L. Luo, Y. R. Lv and Y. H. Xu, One-pot synthesis of peony-like Bi_2S_3/$BiVO_4$ (040) with high photocatalytic activity for glyphosate degradation under visible light irradiation, *Chin. J. Catal.*, 2019, **40**(4), 580–589, DOI: 10.1016/S1872-2067(19)63296-1.

11 I. Teixeira, J. Quiroz, M. Homsi and P. Camargo, An Overview of the Photocatalytic H_2 Evolution by Semiconductor-Based Materials for Nonspecialists, *J. Braz. Chem. Soc.*, 2020, **21**, 211–428, DOI: 10.21577/0103-5053.20190255.

12 E. da Silva, M. de Moraes, W. Brito, R. Passos, R. Brambilla, L. da Costa and L. Pocrifka, Synthesis of ZnO Nanoparticles by the Sol-Gel Protein Route: A Viable and Efficient Method for Photocatalytic Degradation of Methylene Blue and Ibuprofen, *J. Braz. Chem. Soc.*, 2020, DOI: 10.21577/0103-5053.20200050.

13 G. Yu, F. Hu, W. Cheng, Z. Han, C. Liu and Y. Dai, ZnCuAl-LDH/Bi_2 MoO_6 Nanocomposites with Improved Visible Light-Driven Photocatalytic Degradation, *Acta Phys.-Chim. Sin.*, 2020, **36**, 1911016, DOI: 10.3866/PKU.WHXB201911016.

14 S. Li, C. Wang, M. Cai, F. Yang, Y. Liu, J. Chen and X. Chen, Facile fabrication of TaON/Bi_2MoO_6 core-shell S-scheme heterojunction nanofibers for boosting visible-light catalytic levofloxacin degradation and Cr (VI) reduction, *Chem. Eng. J.*, 2021, **131158**, DOI: 10.1016/j.cej.2021.131158.

15 A. Fujishima and K. Honda, Electrochemical Photolysis of Water at a Semiconductor Electrode, *Nature*, 1972, **238**, 37–38, DOI: 10.1038/238037a0.

16 A. L. Linsebigler, G. Lu and J. T. Yates, Photocatalysis on TiO_2 Surfaces: Principles, Mechanisms, and Selected Results, *Chem. Rev.*, 1995, **95**, 735–758, DOI: 10.1021/cr00035a013.

17 W. Y. Teoh, J. A. Scott and R. Amal, Progress in Heterogeneous Photocatalysis: From Classical Radical Chemistry to Engineering Nanomaterials and Solar Reactors, *J. Phys. Chem. Lett.*, 2012, **3**, 629–639, DOI: 10.1021/jz3000646.

18 M. Litter, Heterogeneous photocatalysis Transition metal ions in photocatalytic systems, *Appl. Catal., B*, 1999, **23**, 89–114, DOI: 10.1016/S0926-3373(99)00069-7.

19 J. Wen, X. Li, W. Liu, Y. Fang, J. Xie and Y. Xu, Photocatalysis fundamentals and surface modification of TiO_2 nanomaterials, *Chinese J. Catal.*, 2015, **36**, 2049–2070, DOI: 10.1016/S1872-2067(15)60999-8.

20 K. H. Hama Aziz, K. M. Omer, A. Mahyar, H. Miessner, S. Mueller and D. Moeller, Application of Photocatalytic Falling Film Reactor to Elucidate the Degradation Pathways of Pharmaceutical Diclofenac and Ibuprofen in Aqueous Solutions, *Coatings*, 2019, **9**, 465, DOI: 10.3390/coatings9080465.

21 Z. Wang, V. Srivastava, I. Ambat, Z. Safaei and M. Sillanpää, Degradation of Ibuprofen by UV-LED/catalytic advanced oxidation process, *J. Water Process. Eng.*, 2019, **31**, 100808, DOI: 10.1016/j.jwpe.2019.100808.

22 P. Wang, L. Bu, Y. Wu, W. Ma, S. Zhu and S. Zhou, Mechanistic insight into the degradation of ibuprofen in UV/H_2O_2 process *via* a combined experimental and DFT study, *Chemosphere*, 2021, **267**, 128883, DOI: 10.1016/j.chemosphere.2020.128883.

23 L. Lin, W. Jiang, M. Bechelany, M. Nasr, J. Jarvis, T. Schaub and P. Xu, Adsorption and photocatalytic oxidation of ibuprofen using nanocomposites of TiO_2 nanofibers combined with BN nanosheets: Degradation products and mechanisms, *Chemosphere*, 2019, **220**, 921–929, DOI: 10.1016/j.chemosphere.2018.12.184.

24 J. C. C. Da Silva, J. A. R. Teodoro, R. J. D. C. F. Afonso, S. F. Aquino and R. Augusti, Photolysis and photocatalysis of ibuprofen in aqueous medium: Characterization of by-products *via* liquid chromatography coupled to high-resolution mass spectrometry and assessment of their toxicities against Artemia Salina, *J. Mass Spectrom.*, 2014, **49**, 145–153, DOI: 10.1002/jms.3320.

25 S. Khalaf, J. H. Shoqeir, F. Lelario, S. A. Bufo, R. Karaman and L. Scrano, TiO_2 and Active Coated Glass Photodegradation of Ibuprofen, *Catalysts*, 2020, **10**, 560, DOI: 10.3390/catal10050560.

26 O. O. Wahab, L. O. Olasunkanmi, K. K. Govender and P. P. Govender, A DFT Study of Disperse Yellow 119 Degradation Mechanism by Hydroxyl Radical Attack, *ChemistrySelect*, 2018, **3**, 12988–12997, DOI: 10.1002/slct.201802904.

27 M. Carrier, C. Guillard, M. Besson, C. Bordes and H. Chermette, Photocatalytic Degradation of Diuron: Experimental Analyses and Simulation of HO° Radical Attacks by Density Functional Theory Calculations, *J. Phys. Chem. A*, 2009, **113**, 6365–6374, DOI: 10.1021/jp810146v.

28 A. Romeiro, M. E. Azenha, M. Canle, V. H. N. Rodrigues, J. P. Da Silva and H. D. Burrows, Titanium Dioxide Nanoparticle Photocatalysed Degradation of Ibuprofen and Naproxen in Water: Competing Hydroxyl Radical Attack and Oxidative Decarboxylation by Semiconductor Holes, *ChemistrySelect*, 2018, **3**, 10915–10924, DOI: 10.1002/slct.201801953.

29 R. A. Young, A. Sakthivel, T. S. Moss and C. O. Paiva-Santos, DBWS -9411 – an upgrade of the DBWS *.* programs for Rietveld refinement with PC and mainframe computers, *J. Appl. Crystallogr.*, 1995, **28**, 366–367, DOI: 10.1107/S0021889895002160.

30 G. R. Meima and P. G. Menon, Catalyst deactivation phenomena in styrene production, *Appl. Catal., A*, 2001, **212**, 239–245, DOI: 10.1016/S0926-860X(00)00849-8.

31 A. C. Larson and R. B. Von Dreele, *Gsas General Structure Analysis System*, 86th edn, 2004.

32 B. H. Toby, EXPGUI, a graphical user interface for GSAS, *J. Appl. Crystallogr.*, 2001, **34**, 210–213, DOI: 10.1107/S0021889801002242.

33 P. F. Lindley and D. S. Moss, Elements of X-ray crystallography by L. V. Azaroff, *Acta Crystallogr., Sect. A: Found. Crystallogr.*, 1970, **26**, 701, DOI: 10.1107/S0567739470001808.

34 B. D. Viezbicke, S. Patel, B. E. Davis and D. P. Birnie, Evaluation of the Tauc method for optical absorption edge determination: ZnO thin films as a model system, *Phys. Status Solidi B*, 2015, DOI: 10.1002/pssb.201570351.

35 S. Brunauer, P. H. Emmett and E. Teller, Adsorption of gases in multimolecular layers, *J. Am. Chem. Soc.*, 1938, **60**, 309–319, DOI: 10.1021/ja01269a023.

36 M. Thommes, K. Kaneko, A. V Neimark, J. P. Olivier, F. Rodriguez-Reinoso, J. Rouquerol and K. S. W. Sing, Physisorption of gases, with special reference to the evaluation of surface area and pore size distribution (IUPAC Technical Report), *Pure Appl. Chem.*, 2015, **87**, 1051–1069.

37 J. Rouquerol and F. Rouquerol, 3 methodology of gas adsorption, in *Adsorpt. By Powders Porous Solids*, ed. F. Rouquerol, J. Rouquerol, K. S. W. Sing, P. Llewellyn and G. Maurin, Academic Press, 2nd edn, Oxford, 2014, pp. 57–104, DOI: DOI: 10.1016/B978-0-08-097035-6.00003-6.

38 C. Lee, W. Yang and R. G. Parr, Development of the Colle-Salvetti correlation-energy formula into a functional of the electron density, *Phys. Rev. B*, 1988, **37**, 785–789, DOI: 10.1103/PhysRevB.37.785.

39 S. Grimme, S. Ehrlich and L. Goerigk, Effect of the damping function in dispersion corrected density functional theory, *J. Comput. Chem.*, 2011, **32**, 1456–1465, DOI: 10.1002/jcc.21759.

40 T. Yanai, D. P. Tew and N. C. Handy, A new hybrid exchange–correlation functional using the Coulomb-attenuating method (CAM-B3LYP), *Chem. Phys. Lett.*, 2004, **393**, 51–57, DOI: 10.1016/j.cplett.2004.06.011.

41 J. P. Perdew, Density-functional approximation for the correlation energy of the inhomogeneous electron gas, *Phys. Rev. B*, 1986, **33**, 8822–8824, DOI: 10.1103/PhysRevB.33.8822.

42 J.-D. Chai and M. Head-Gordon, Long-range corrected hybrid density functionals with damped atom–atom dispersion corrections, *Phys. Chem. Chem. Phys.*, 2008, **10**, 6615, DOI: 10.1039/b810189b.

43 R. Peverati and D. G. Truhlar, An improved and broadly accurate local approximation to the exchange–correlation density functional: The MN12-L functional for electronic structure calculations in chemistry and physics, *Phys. Chem. Chem. Phys.*, 2012, **14**, 13171, DOI: 10.1039/c2cp42025b.

44 R. Peverati and D. G. Truhlar, Screened-exchange density functionals with broad accuracy for chemistry and solid-state physics, *Phys. Chem. Chem. Phys.*, 2012, **14**, 16187, DOI: 10.1039/c2cp42576a.

45 J. P. Perdew, K. Burke and M. Ernzerhof, Generalized Gradient Approximation Made Simple, *Phys. Rev. Lett.*, 1996, **77**, 3865–3868, DOI: 10.1103/PhysRevLett.77.3865.

46 C. Adamo and V. Barone, Exchange functionals with improved long-range behavior and adiabatic connection methods without adjustable parameters: The mPW and mPW1PW models, *J. Chem. Phys.*, 1998, **108**, 664–675, DOI: 10.1063/1.475428.

47 J. Tao, J. P. Perdew, V. N. Staroverov and G. E. Scuseria, Climbing the Density Functional Ladder: Nonempirical Meta–Generalized Gradient Approximation Designed for Molecules and Solids, *Phys. Rev. Lett.*, 2003, **91**, 146401, DOI: 10.1103/PhysRevLett.91.146401.

48 V. N. Staroverov, G. E. Scuseria, J. Tao and J. P. Perdew, Comparative assessment of a new nonempirical density functional: Molecules and hydrogen-bonded complexes, *J. Chem. Phys.*, 2003, **119**, 12129–12137, DOI: 10.1063/1.1626543.

49 V. A. Rassolov, M. A. Ratner, J. A. Pople, P. C. Redfern and L. A. Curtiss, 6-31G* basis set for third-row atoms, *J. Comput. Chem.*, 2001, **22**, 976–984, DOI: 10.1002/jcc.1058.

50 A. L. Romero, L. H. B. Baptistella, F. Coelho and P. M. Imamura, Resolução do ibuprofeno: um projeto para disciplina de química orgânica experimental, *Quim. Nova*, 2012, **35**, 1680–1685, DOI: 10.1590/S0100-40422012000800031.

51 M. J. Frisch, G. W. Trucks, H. B. Schlegel, G. E. Scuseria, M. A. Robb, J. R. Cheeseman, G. Scalmani, V. Barone, B. Mennucci, G. A. Petersson, H. Nakatsuji, M. Caricato, X. Li, H. P. Hratchian, A. F. Izmaylov, J. Bloino, G. Zheng, J. L. Sonnenberg, M. Hada, M. Ehara, K. Toyota, R. Fukuda, J. Hasegawa, M. Ishida, T. Nakajima, Y. Honda, O. Kitao, H. Nakai, T. Vreven, J. A. Montgomery Jr, J. E. Peralta, F. Ogliaro, M. Bearpark, J. J. Heyd, E. Brothers, K. N. Kudin, V. N. Staroverov, R. Kobayashi, J. Normand, K. Raghavachari, A. Rendell, J. C. Burant, S. S. Iyengar, J. Tomasi, M. Cossi, N. Rega, J. M. Millam,

M. Klene, J. E. Knox, J. B. Cross, V. Bakken, C. Adamo, J. Jaramillo, R. Gomperts, R. E. Stratmann, O. Yazyev, A. J. Austin, R. Cammi, C. Pomelli, J. W. Ochterski, R. L. Martin, K. Morokuma, V. G. Zakrzewski, G. A. Voth, P. Salvador, J. J. Dannenberg, S. Dapprich, A. D. D. Farkas, J. B. Foresman, J. V Ortiz, J. Cioslowski and D. J. Fox, *Gaussian 09 Revision D.01*, Gaussian Inc. Wallingford CT, Gaussian 09 Revis. C.01, 2010.

52 M. Xu, Y. Gao, E. M. Moreno, M. Kunst, M. Muhler, Y. Wang, H. Idriss and C. Wöll, Photocatalytic Activity of Bulk TiO_2 Anatase and Rutile Single Crystals Using Infrared Absorption Spectroscopy, *Phys. Rev. Lett.*, 2011, **106**, 138302, DOI: 10.1103/PhysRevLett.106.138302.

53 N. Abdullah, B. V. Ayodele, W. N. W. Mansor and S. Abdullah, Effect of incorporating TiO_2 photocatalyst in PVDF hollow fibre membrane for photo-assisted degradation of methylene blue, *Bull. Chem. React. Eng. Catal.*, 2018, **13**(3), 588–591, DOI: 10.9767/bcrec.13.3.2909.588-591.

54 M. O. Miranda, W. E. C. l Cavalcanti, F. I. da Silva, E. Rigoti, E. R. Castellón, S. B. C. Pergher and T. P. Braga, Photocatalytic degradation of ibuprofen using modified titanium oxide supported on CMK-3: effect of Ti content on the TiO_2 and carbon interaction, *Catal. Sci. Technol.*, 2020, **10**, 7681–7696, DOI: 10.1039/d0cy01167c.

55 H. Ennaceri, M. Boujnah, A. Taleb, A. Khaldoun, R. Sáez-Araoz, A. Ennaoui, A. El Kenz and A. Benyoussef, Thickness effect on the optical properties of TiO_2-anatase thin films prepared by ultrasonic spray pyrolysis: Experimental and *ab initio* study, *Int. J. Hydrogen Energy*, 2017, **42**, 19467–19480, DOI: 10.1016/j.ijhydene.2017.06.015.

56 P. Iovino, S. Chianese, S. Canzano, M. Prisciandaro and D. Musmarra, Degradation of Ibuprofen in Aqueous Solution with UV Light: the Effect of Reactor Volume and pH, *Water, Air, Soil Pollut.*, 2016, **227**, 194, DOI: 10.1007/s11270-016-2890-3.

57 H. Zhang, P. Zhang, Y. Ji, J. Tian and Z. Du, Photocatalytic degradation of four non-steroidal anti-inflammatory drugs in water under visible light by P25-TiO_2/tetraethyl orthosilicate film and determination *via* ultra performance liquid chromatography electrospray tandem mass spectrometry, *Chem. Eng. J.*, 2015, **262**, 1108–1115, DOI: 10.1016/j.cej.2014.10.019.

58 J. Choina, H. Kosslick, C. Fischer, G.-U. Flechsig, L. Frunza and A. Schulz, Photocatalytic decomposition of pharmaceutical ibuprofen pollutions in water over titania catalyst, *Appl. Catal., B*, 2013, **129**, 589–598, DOI: 10.1016/j.apcatb.2012.09.053.

59 K. Suttiponparnit, J. Jiang, M. Sahu, S. Suvachittanont, T. Charinpanitkul and P. Biswas, Role of Surface Area, Primary Particle Size, and Crystal Phase on Titanium Dioxide Nanoparticle Dispersion Properties, *Nanoscale Res. Lett.*, 2011, **6**, 27, DOI: 10.1007/s11671-010-9772-1.

60 G. A. Parks, The Isoelectric Points of Solid Oxides, Solid Hydroxides, and Aqueous Hydroxo Complex Systems, *Chem. Rev.*, 1965, **65**, 177–198, DOI: 10.1021/cr60234a002.

61 A. Surenjan, T. Pradeep and L. Philip, *Chemosphere*, 2019, **228**, 629–639.

62 V. Polliotto, F. R. Pomilla, V. Maurino, G. Marcì, A. Bianco Prevot, R. Nisticò, G. Magnacca, M. C. Paganini, L. Ponce Robles, L. Perez and S. Malato, *Catal. Today*, 2019, **328**, 164–171.

63 T. M. Khedr, S. M. El-Sheikh, A. A. Ismail and D. W. Bahnemann, *Opt. Mater.*, 2018, **88**, 117–127, DOI: 10.1016/j.optmat.2018.11.027.

64 N. Jallouli, L. M. Pastrana-Martínez, A. R. Ribeiro, N. F. Moreira, J. L. Faria, O. Hentati and M. Ksibi, Heterogeneous photocatalytic degradation of ibuprofen in ultrapure water, municipal and pharmaceutical industry wastewaters using a TiO_2/UV-LED system, *Chem. Eng. J.*, 2018, **334**, 976–984.

65 X. Yao, X. Hu, Y. Liu, X. Wang, X. Hong, X. Chen and D. Wang, Simultaneous photocatalytic degradation of ibuprofen and H_2 evolution over Au/sheaf-like TiO2 mesocrystals, *Chemosphere*, 2020, **261**, 127759.

66 M. Tanveer, G. T. Guyer and G. Abbas, Photocatalytic degradation of ibuprofen in water using TiO_2 and ZnO under artificial UV and solar irradiation, *Water Environ. Res.*, 2019, **91**(9), 822–829.

67 W. C. Cory, C. Harris and S. Martinez, Accelerated degradation of ibuprofen in tablets, *Pharm. Dev. Technol.*, 2010, **15**, 636–643, DOI: 10.3109/10837450903426518.

68 X. Liu, Z. Guo, L. Zhou, J. Yang, H. Cao, M. Xiong, Y. Xie and G. Jia, Hierarchical biomimetic $BiVO_4$ for the treatment of pharmaceutical wastewater in visible-light photocatalytic ozonation, *Chemosphere*, 2019, **222**, 38–45, DOI: 10.1016/j.chemosphere.2019.01.084.

69 A. Núñez-Flores, A. Sandoval, E. Mancilla, A. Hidalgo-Millán and G. Ascanio, Enhancement of photocatalytic degradation of ibuprofen contained in water using a static mixer, *Chem. Eng. Res. Des.*, 2020, **156**, 54–63, DOI: 10.1016/j.cherd.2020.01.018.

70 K. Krumova and G. Cosa, *Overview of Reactive Oxygen Species*, in: n.d., pp. 1–21, ch 1, DOI: DOI: 10.1039/9781782622208-00001.

71 G. R. Buettner, The Pecking Order of Free Radicals and Antioxidants: Lipid Peroxidation, α-Tocopherol, and Ascorbate, *Arch. Biochem. Biophys.*, 1993, **300**, 535–543, DOI: 10.1006/abbi.1993.1074.

72 G. Liu, Recalcitrance of cyanuric acid to oxidative degradation by OH radical: theoretical investigation, *RSC Adv.*, 2014, **4**, 37359–37364, DOI: 10.1039/c4ra04687k.

73 R. Mohammadi, B. Massoumi and M. Rabani, Photocatalytic decomposition of amoxicillin trihydrate antibiotic in aqueous solutions under UV irradiation using Sn/TiO2 nanoparticles, *Int. J. Photoenergy*, 2012, 1–11.

74 X. Li, R. Xiong and G. Wei, Preparation and photocatalytic activity of nanoglued Sn-doped TiO_2, *J. Hazard. Mater.*, 2009, **164**(2–3), 587–591.

75 R. S. Lankone, A. R. Deline, M. Barclay and D. H. Fairbrother, UV-vis quantification of hydroxyl radical concentration and dose using principal component analysis, *Talanta*, 2020, **218**, 121148.